Bidirectional transport by molecular motors: Enhanced processivity and response to external forces - Supplementary material -

Melanie J. I. Müller, Stefan Klumpp, and Reinhard Lipowsky,
Max Planck Institute of Colloids and Interfaces, Potsdam, Germany

S1   Tug-of-war model

In this section we review the details of our theoretical description introduced in Refs. (1, 2), and discuss our choices for the force-dependence of the motor rates.

S1.1   Single motor properties

Our theory is based on single motor properties as briefly summarized in Section 2 of the main text, and described in more detail here. Each motor binds to the filament, walks along it, and unbinds from it stochastically with force-dependent rates derived from single molecule experiments. In these experiments, the motor moves against a load force F exerted by an optical trap.

Unbinding rate. The motor unbinding rate has been measured to increase approximately exponentially for kinesin-1 (3),

$$\epsilon(F) = \epsilon_0 \exp\left[F/F_d\right], \tag{S1}$$

where the force scale is given by the detachment force F_d. Such an exponential increase is also expected on theoretical grounds from Kramers theory (4), or its application by Bell (5).

Velocity. The motor velocity decreases with the load force and crosses zero at the stall force F_s. The exact functional form of the force-velocity curve depends on the precise experimental conditions, notably the ATP concentration (3, 6–9). For simplicity, we use a piecewise linear force-dependence for the average motor velocity as given by

$$v(F) = \begin{cases} v_F\left(1 - F/F_s\right) & \text{for } 0 \leq F \leq F_s \text{ (forward)} \\ v_B\left(1 - F/F_s\right) & \text{for } F > F_s \text{ (backward)} \end{cases}, \tag{S2}$$

see the blue curve in Fig. S1(a). For substall forces, $F < F_s$, the linear decrease is often a good approximation under high ATP concentrations (6, 7), although deviations from linearity have also been reported (3, 8, 9). For superstall load forces $F > F_s$, the motor walks backwards, but only slowly, as has been shown for kinesin 1 (9, 10) and cytoplasmic dynein (11, 12). The precise form of the force-velocity curve in the superstall regime is unclear (9), although theoretical considerations indicate that it might exhibit a shallow minimum (13, 14). The only important feature of the superstall velocity for our model is its small magnitude. In this range, our linear force-velocity relation (S2) can be considered as a Taylor expansion to first order in $F - F_s$, where the small backward motion is taken into account by using a small backward velocity parameter, $v_B \ll v_F$.
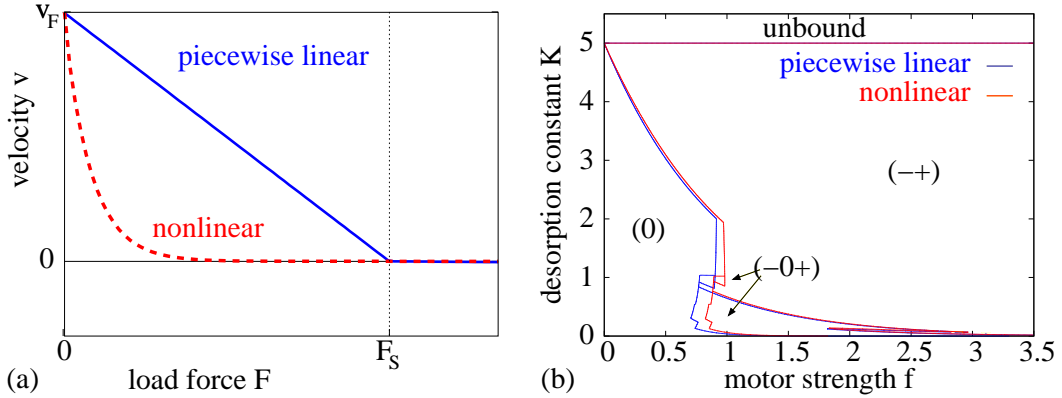
Figure S1: (a) Comparison of two different force-velocity-relations: Relation (S2) (blue solid line) and nonlinear relation (S14) (red dashed line), using the kinesin-1 parameters of Table S1 and $F_v = 0.5\,\mathrm{pN}$. (b) Motility diagram for the symmetric tug-of-war of $N_+ = N_- = 5$ motors with the piecewise linear force-velocity curve (blue lines) and the nonlinear force velocity curve (red lines). Parameters are as in (a), except for the variable parameters stall force F_s and unbinding rate ϵ_0.

Apart from being a good approximation for the experimental force-velocity curve, the piecewise-linear force-velocity curve (S2) allows to derive explicit expression for the cargo force and velocity, see Section S1.2 below. Furthermore, while nonlinearities in the force-velocity curve can provide insight into the underlying motor mechanism (13–16), our results do not depend crucially on the precise form of the force-velocity relation, as long as it decreases monotonically and has a small superstall backward velocity, as we show below in Section S1.4.

In order to simplify our notation, we rewrite the force-velocity-relationship (S2) as

$$v(F) = v_o \left(1 - F/F_s\right), \tag{S3}$$

where we have defined the convenient velocity parameter

$$v_o \equiv v_F \text{ for } 0 \le F \le F_s, \text{ and } v_o \equiv v_B \text{ for } F > F_s. \tag{S4}$$

Binding rate. The force-dependence of the binding rate is difficult to access experimentally. However, it should depend only weakly on the load force, since an unbound motor relaxes and then binds from its relaxed state, see also the discussion in Ref. (17). We therefore assume the binding rate to be independent of the load force,

$$\pi(F) = \pi_0. \tag{S5}$$

Vectorial character of the force. In the single motor experiments used to determine the single motor rates (S1-S3), the stepping motor is attached to a bead to which a force F_{trap} is applied using an optical trap. Although perpendicular trapping forces have also been used (18), in the standard trapping experiments relevant here the direction of F_{trap} is chosen to be parallel to the filament, as explained in Ref. (6). The motor velocities or run lengths are recorded as functions of F_{trap}. Therefore, the force F that enters in our relations (S1-S3) as well as in Equation (1) of the main text is identical with the force F_{trap} parallel to the filament.

In general, the bead experiences both the longitudinal force F_{trap} and a force $F_\perp$ perpendicular to the filament, the latter arising from the interactions of the bead with the filament and/or with the surface, on which this filament has been immobilized (6). The two forces F_{trap}

and $F_\perp$ are transduced to the stalk of the motor and are then balanced by opposing forces that are generated by the motor. In principle, the perpendicular force $F_\perp$ could be determined experimentally by measuring the angle, say θ, between the motor stalk and the filament, since $F_\perp = F_{\text{trap}} \tan(\theta)$. In practice, this angle is not accessible using the available experimental techniques, and the magnitude of the perpendicular force component $F_\perp$ has not been measured in the optical trap experiments addressed here. From the theoretical point of view, the perpendicular component $F_\perp$, has been proposed to play an important role for the force-dependent motor movements and the chemomechanical cycle of molecular motors (19, 20). It has also been emphasized in Ref. (21) that the motor does not expend work against the perpendicular force component $F_\perp$ even though this parameter enters the transition rates between the different motor states.

For bidirectional transport as studied here, two motor teams, denoted as plus and minus motors, pull on the cargo. As in the single motor experiments, the plus and the minus motors generate both longitudinal and perpendicular force components. The latter force components are again balanced by interactions between the cargo and the filament. Therefore, the force balance between these two motor teams as described in the next subsection depends only on the longitudinal force components generated by the two types of motors. Furthermore, since the perpendicular force between cargo and filament is shared by all motors, the perpendicular force acting on each motor individually is expected to be relatively small.

S1.2   Cargo forces and velocities

We consider a cargo transported by a fixed number of N_+ plus and N_- minus motors. As the motors stochastically bind to and unbind from the filament, only n_+ plus and n_- minus motors are bound to the filament at a given time, with $0 \le n_+ \le N_+$ and $0 \le n_- \le N_-$. These numbers (n_+, n_-) change when a motor binds or unbinds.

Rates for motor binding and unbinding. The rates for these events are determined by the single motor rates described in Section S1.1 and by the load forces F_+ and $-F_-$ on each plus and on each minus motor, respectively, where the sign of the force is chosen positive if it points into the minus direction. This implies that the effective rate for the unbinding of one plus motor in the cargo state (n_+, n_-) is

$$\epsilon_+(n_+, n_-) = n_+ \, \epsilon_{0+} \, \exp\left[F_+/F_{d+}\right]. \tag{S6}$$

The prefactor n_+ in Equation (S6) describes that there are n_+ bound plus motors available for unbinding. Similarly, the effective rate for the binding of one plus motor in the state (n_+, n_-), where there are $(N_+ - n_+)$ unbound plus motors, is

$$\pi_+(n_+, n_-) = (N_+ - n_+) \, \pi_{0+}. \tag{S7}$$

Analogous expressions hold for the unbinding and binding rates of a single minus motor, with the '+' indices replaced by '−' indices. The load forces F_+ and $-F_-$ on the plus and minus motors are determined by assumption (1) of Section 2, which in mathematical terms becomes the force balance

$$n_+ F_+ = -n_- F_- \tag{S8}$$

for a cargo pulled by n_+ plus and n_- minus motors. Furthermore, assumption (2) states that the plus and minus motors must move with the same velocity, which is identical to the velocity v_c of their common cargo:

$$v_c(n_+, n_-) \equiv v_+(F_+) = -v_-(-F_-). \tag{S9}$$

Here, the sign of the velocity is taken to be positive in the plus direction. The force and velocity balances as given by equations (S8) and (S9) lead to the cargo velocity

$$v_c(n_+, n_-) \;\; = \;\; \frac{F_{s+} n_+ - F_{s+} n_-}{n_+ F_{s+}/v_{o+} + n_- F_{s-}/v_{o-}} \tag{S10}$$

and to the motor forces

$$n_+ F_+ = -n_- F_- = \frac{(1/v_{o+} + 1/v_{o-})\, n_+ n_- F_{s+} F_{s-}}{n_+ F_{s+}/v_{o+} + n_- F_{s-}/v_{o-}}. \tag{S11}$$

Here, the velocity parameters v_{o+} and v_{o-} have to be replaced by the corresponding forward or backward velocities according to Equation (S4) and the 'majority rule'

$$
\begin{aligned}
v_c > 0 & \quad \text{if } F_{s+} n_+ > F_{s-} n_- \text{ (plus motors 'win')} \\
v_c < 0 & \quad \text{if } F_{s+} n_+ < F_{s-} n_- \text{ (minus motors 'win')} \\
v_c = 0 & \quad \text{if } F_{s+} n_+ = F_{s-} n_- \text{ ('tie')},
\end{aligned}
\tag{S12}
$$

in agreement with Equation (S10). Equation (S11) defines a 'cargo force'

$$F_c(n_+, n_-) \equiv n_+ F_+ = -n_- F_-. \tag{S13}$$

In our tug-of-war model, the motors interact with each other only because of the mechanical coupling via their common cargo. There is no 'coordination complex' which coordinates their motion. This means that cellular regulation can affect the cargo motion only by influencing the motor properties such as the filament affinity or the stall force. In the absence of such regulation, the cargo will exhibit fast bidirectional motion on its own.

Simulation. With the motor forces given in Equation (S11), the rates (S6-S7) and the analogous equations for the minus motors determine a Markov process on the two-dimensional state space (n_+, n_-) of bound plus and minus motors, corresponding to a Master equation for the probability $p(n_+, n_-, t)$ to have n_+ active plus and n_- active minus motors at time t. The explicit Master equation is given in Ref. (2). Since experiments usually monitor only cargos which are bound to the filament, and which have been walking along this filament for some (unknown) time, we are interested in the stationary state solution $p(n_+, n_-)$ of this Master equation, see Refs. (1, 2) for details. We solve the Master equation for the steady state by determining the eigenvector of the associated transition matrix with eigenvalue zero (4). In addition, we simulate individual cargo trajectories by using the Gillespie algorithm (22) for the binding/unbinding dynamics given by Equations (S6-S7) and the analogous equation for the minus motors, and let the cargo move with velocity v_c from Equation (S10) in the intervals between (un-)binding events.

Parameter estimation. In our tug-of-war model, a single motor is described by the six parameters F_s, F_d, ϵ_0, π_0, v_F and v_B, which are all accessible to single molecule experiments in principle. We have used results from such experiments when available. For kinesin-1, all parameters have been measured. From single molecule optical trapping, the stall force has been directly measured as $F_s \approx 6\,\text{pN}$ (3, 6). The detachment force $F_d \approx 3\,\text{pN}$ can be estimated from the dependence of the run length on the trapping force (3). The unbinding rate has been reported of the order of $\epsilon_0 \approx 1/\text{s}$ (3, 23) , while the binding rate $\pi_0 \approx 5/\text{s}$ was obtained from fitting of experimental data (24, 25). Kinesin forward velocities were found in the range of $v_F \approx 1\,\mu\text{m/s}$ (9, 26). The backward velocity v_B characterizes the slope v_B/F_s of the force-velocity relation for superstall forces $F > F_s$, see Equation (S2), and was estimated from the superstall part of the force-velocity-curve of Ref. (9) as $v_B \approx 6\,\text{nm/s}$.

Parameter	Symbol	Kinesin	Dynein
Stall force	F_s	6 pN	7 pN
Detachment force	F_d	3 pN	3 pN
Unbinding rate	ϵ_0	1/s	0.25/s
Binding rate	π_0	5/s	1.5/s
Forward velocity	v_F	1 μm/s	1 μm/s
Backward velocity	v_B	6 nm/s	6 nm/s

Table S1: Single motor parameters of our model, and values for kinesin-1 (kinesin) and cytoplasmic dynein (dynein), see text for references.

For cytoplasmic dynein, we chose to work with a stall force of $F_s \approx 7$ pN as reported in Ref. (27), although much smaller values $F_s \approx 1$ pN have also been found (28). We obtained the dynein unbinding rate $\epsilon_0 \approx 0.25$/s from Ref. (23, 29) and the forward velocity $v_F \approx 1\,\mu$m/s from Ref. (23, 27). The binding rate was estimated as described in Ref. (30) as $\pi_0 \approx 1.5$/s, using the equilibrium desorption constant $K_{\mathrm{MT}} \approx 0.5\,\mu$M (23, 29), and the unbinding rate $\epsilon_0 \approx 0.25$/s. No estimate for the slope of the force-velocity relation in the superstall regime was available. Therefore we used the same value as for kinesin-1, $v_F = 6$ nm/s. We note that some observations suggest that the backward velocity of dynein is higher than that of kinesin (28, 31). In our model, however, the precise value of the backward velocity parameter does not change the cargo motion significantly as long as v_B is well below 10% of the forward velocity v_F, see Fig. 2(b). Even if dynein motors move backward ten times faster that kinesins, this condition is still satisfied.

The parameters for kinesin and dynein are summarized in Table S1.

S1.3 Motility states of the cargo

As described in our earlier publications (1, 2), cargo transport described by the above stochastic tug-of-war model can exhibit up to 7 different motility patterns, depending on the parameters of the involved motors. These 'motility states' are characterized by distinct patterns of maxima in the probability distribution $p(n_+, n_-)$ for the numbers of bound plus and minus motors.

For a symmetric tug-of-war of $N = N_+ = N_-$ plus and minus motors which differ only in their forward direction, the number of motility states is reduced from seven to three.

Strong motors with a high stall to detachment force ratio can produce a larger force than they can sustain, and can thus pull each other off the filament. This leads to an unbinding cascade of one team of motors as described in the main text and Refs. (1, 2), and thus to a low probability of states with both types of motors bound. The probability distribution $p(n_+, n_-)$ to have n_+ plus and n_- minus motors bound exhibits two probability peaks at $(n_+, n_-) = (n, 0)$ and $(n_+, n_-) = (0, n)$, corresponding to fast plus and fast minus motion, respectively. Switching between these two high-probability states leads to fast bidirectional motion, the $(-+)$ motility state.

Weak motors with a small stall to detachment force ratio can produce only a small force compared to the force that they can sustain. In consequence, the motors do not significantly feel each other, so that they randomly bind to and unbind from the filament. This leads to a high probability for a state $(n_+, n_-) = (n, n)$, where n is determined by the binding affinity of the motors. The motors thus block each other, and the cargo exhibits only slow motility, which defines the no-motion motility state (0).

In the intermediate case of motors with comparable stall and detachment forces, all three types of maxima appear, and the cargo is in the $(-0+)$ motility state of fast bidirectional motion interrupted by pauses.

For an asymmetric tug-of-war with different numbers and/or parameters of plus and minus motors, all combinations of fast plus motion, fast minus motion and pauses are possible, leading to the 7 motility states $(+)$, $(-)$, (0), $(-+)$, $(0+)$, (-0), and $(-0+)$.

In this article, we focus on the motility state $(-+)$ of fast bidirectional motion, as exhibited by a cargo transported by two teams of strong motors.

S1.4 The shape of the single motor force-velocity relation

In this section we investigate the effect of the shape of the force-velocity curve on our results. Thus, we consider the same tug-of-war model as before, but use a force-velocity relationship that differs from Equation (S2). We chose the relationship

$$v(F) = v_F \frac{e^{-F/F_v} - e^{-F_s/F_v}}{1 - e^{-F_s/F_v}} \tag{S14}$$

as proposed in Ref. (32), where $F_v = k_{\mathrm{B}}T/l$ is the characteristic force associated with the step size l. For microtubule motors at room temperature, one has $l = 8\,\mathrm{nm}$ and $F_v = 0.5\,\mathrm{pN}$. Equation (S14) provides a simple example for a strongly nonlinear force-velocity curve which exhibits the major characteristics of experimental force-velocity curves, namely a monotonic decrease with force in the substall regime and small negative velocities in the superstall regime, see Fig. S1(a). For kinesin parameters, this nonlinear force-velocity curve (S14) looks quite different from our piecewise linear force-velocity curve (S2). With the nonlinear force-velocity relation (S14), the equations for the motor forces, Equations (S8) and (S9), are transcendental and cannot be solved analytically. We therefore determined the forces numerically using Ridder's method (33).

Fig. S1(b) shows the motility diagrams of the symmetric tug-of-war of $N_+ = N_- = 5$ plus and minus kinesin-like motors, both with the piecewise linear force-velocity curve (S2) (blue lines) and the nonlinear force-velocity curve (S14) (red lines). The two motility diagrams look very similar; the main difference is that the transition lines for the diagram with the nonlinear force-velocity relation are shifted a bit to higher motor forces f. The reason is that the nonlinear force-velocity relation (S14) decreases very fast to low velocities, see Fig. S1(a), which has the same effect as a lower stall force F_s or a lower motor strength f.

Analogous effects can be observed in the case of the asymmetric tug-of-war of plus and minus motors with different parameters (not shown). In a motility diagram similar to Fig. S1(b), the same seven motility states $(+)$, $(-)$, (0), $(-+)$, $(0+)$, (-0) and $(-0+)$ appear in comparable regions of the parameter space for both force-velocity relations. Only the locations of the transition lines between the motility states are shifted somewhat. As for the symmetric tug-of-war, the effectively lower stall force of the force-velocity-relation (S14) suppresses motor unbinding cascades. Therefore, parameter regions of the 'uncooperative' motility states (0), $(+)$, $(-)$, $(0+)$ and (-0) are increased compared to the piecewise linear force-velocity relation (S2), at the expense of the 'cooperative' motility states $(-+)$ and $(-0+)$.

In summary, the two different force-velocity relations (S2) and (S14) lead to qualitatively similar motility diagrams and, in particular, to the same types of motility states. Our model results therefore do not depend strongly on the exact form of the force-velocity relation, as long as it decreases monotonically with the external force and exhibits slow superstall backward motion.

S2 Run, switch and binding time

In this section we describe how we obtain the run and switch times, length and velocities discussed in Section 3.

Calculation of run and switch times. The most straightforward way is to measure these quantities for each trajectory of our tug-of-war simulation, just as in experiments. However, it is more convenient (faster) to calculate these quantities from the steady state probability $p(n_+, n_-)$ of the Master equation to have n_+ active plus and n_- active minus motors. For example, the average plus run time $t_{R,+}$ is the sojourn time of the random walk in the plus motion states (n_+, n_-) with $F_{s+} n_+ > F_{s-} n_-$, compare Equation (S12). To calculate this time $t_{R,+}$, consider the number of visits to the plus motion states in time T, which equals $T J_+$, where

$$
\begin{aligned}
J_+ = \ & \textstyle\sum_{(n_+-1)F_{s+} \leq n_- F_{s-} < n_+ F_{s+}} p(n_+, n_-)\, \epsilon_+(n_+, n_-) \\
& + \textstyle\sum_{n_- F_{s-} < n_+ F_{s+} \leq (n_-+1)F_{s-}} p(n_+, n_-)\, \pi_-(n_+, n_-)
\end{aligned}
$$

is the total current out of the plus motion states. The total time spent in the plus motion states during time T is $\tau_+ = T\, P_+$ with the probability

$$
P_+ = \sum_{n_+ F_{s+} > n_- F_{s-}} p(n_+, n_-) \tag{S15}
$$

to be in a plus motion state. The sojourn time of the random walk in the plus motion states is obtained from the last two equations as

$$
t_{R,+} = P_+/J_+, \tag{S16}
$$

The plus run length $x_{R,+}$ is obtained from Equations (S15-S16) by substituting

$$
\begin{aligned}
\epsilon_+(n_+, n_-) &\rightarrow \epsilon_+(n_+, n_-)/v_c(n_+, n_-), \text{ and} \\
\pi_-(n_+, n_-) &\rightarrow \pi_-(n_+, n_-)/v_c(n_+, n_-).
\end{aligned} \tag{S17}
$$

The plus run velocity is then given by $v_{R,+} = x_{R,+}/t_{R,+}$. The minus run times, lengths and velocities can be calculated analogously.

Approximation for large motor forces. Here we focus on cargo transport by motors with high stall to detachment force ratio $f = F_s/F_d$. As discussed in Section S1.3, a cargo pulled by such strong motors has a high probability to have only one motor species active at a given time. In an approximation we therefore neglect states with both motor types active, which reduces the possible cargo states to the 'plus motor states' $(n_+, 0)$, $1 \leq n_+ \leq N_+$, with only plus motors bound and cargo velocity v_{F+}, the 'minus motor states' $(0, n_-)$, $1 \leq n_- \leq N_-$ with only minus motors bound and cargo velocity v_{F-}, and the 'unbound state' $(0, 0)$ with no motors bound and cargo velocity zero. Although directional switching in this approximation can occur only via the unbound state $(0, 0)$, we neglect cargo unbinding when calculating run, pause and switch times. This is justified because the switching via $(0, 0)$ in this approximation represents all switching events via states (n_+, n_-) with $n_+ > 0$, $n_- > 0$ of the full model, and because a cargo in the state $(0, 0)$ does not necessarily unbind, compare the discussion in Section 3.2.

After this reduction of the state space, a plus run must start in the state $(n_+, n_-) = (1, 0)$ with only one plus motor bound, then spend some time on the plus motion states $(n_+, 0)$ with $n_+ > 0$, and finally end upon reaching the state $(0, 0)$. The average run time $t_{R,+}$ of this one-dimensional walk is equivalent to the binding time of a cargo transported by N_+ plus and no minus motors, and has been calculated in (17) as

$$
t_{R,+}(N_+) = \left[\left(1 + \tfrac{\pi_{0+}}{\epsilon_{0+}} \right)^{N_+} - 1 \right] \Big/ [N_+ \pi_{0+}]. \tag{S18}
$$

Analogously, the minus run time is

$$t_{R,-}(N_-) = \left[\left(1 + \frac{\pi_{0-}}{\epsilon_{0-}} \right)^{N_-} - 1 \right] \Big/ [N_- \pi_{0-}]. \tag{S19}$$

The approximation (S18) significantly overestimates the run times (not shown) because it neglects directional switches via cargo states (n_+, n_-) with both motors bound, $n_+ > 0$ and $n_- > 0$. However, it gives the correct exponential scaling with the motor numbers N_+, N_-, see below.

Binding time. The binding time is the time from cargo binding to the filament with the first motor until unbinding of the cargo from the filament. It can be determined from simulation trajectories in the same way as from experimental trajectories. We now derive an approximate analytical expression for the binding time. Cargo binding happens with a plus motor with probability

$$q_+ \equiv (N_+ \pi_{0+}) / (N_+ \pi_{0+} + N_- \pi_{0-}) \tag{S20}$$

and with a minus motor with probability $q_- \equiv 1 - q_+$. Cargo unbinding can occur only from the state $(0,0)$ with no motors bound. Here we assume that a cargo always unbinds upon reaching this state. This is a good approximation for *in vitro* experiments, but possibly not for some *in vivo* cargos, see Section 3.2 for a discussion of this point. When having bound with a plus motor, in the one-dimensional approximation introduced above, the cargo spends its bound time on the plus motor states $(n_+, 0)$ and unbinds upon reaching the state $(0,0)$. In this case the average binding time is equal to the average plus run time $t_{R,+}$ of Equation (S18). In the case of cargo binding with a minus motor, the binding time analogously equals the minus run time $t_{R,-}$. The total average binding time is therefore given by the weighted average of the run times $t_{R,+}$ and $t_{R,-}$, i.e. by

$$\Delta t_b(N_+, N_-) = q_+ \, t_{R,+}(N_+) + q_- \, t_{R,-}(N_-). \tag{S21}$$

When inserting the expressions for q_+, q_-, $t_{R,+}$ and $t_{R,-}$ from Equations (S18-S20), one obtains Equation (3) in the main text.

Equation (S21) resp. Equation (3) are very good approximations for the binding time of a cargo transported by two teams of strong molecular motors, as can be seen in Fig. 2(a) and (c) as well as in Fig. 3(a). In the case of a symmetric tug-of-war, the plus and minus run times are identical, $t_{R,+} = t_{R,-} = t_R$, and the plus and minus runs occur with equal frequency, $q_+ = q_- = 1/2$. Therefore, the approximations for the binding time as given by Equation (S21) resp. Equation (3), and for the run times as in Equations (S18) and (S19) lead to identical results, $\Delta t_b = t_R$. In contrast, the stochastic simulations show that the binding time Δt_b is always larger than the run time t_R, see Fig. 2(a) and (c). Therefore, the approximation (S18) for the run time overestimates the actual run time. The reason for this overestimation is as follows: As explained above, a cargo transported by two teams of strong motors spends most of its time in the plus motion states $(n_+, 0)$ and the minus motion states $(0, n_-)$. Thus, excursions into the pausing states (n_+, n_-) with $n_+ > 0$ and $n_- > 0$ are very short. Since such excursions are both short and do not lead to cargo unbinding, their effect on the cargo binding time is negligible, so that Equation (S21) resp. Equation (3) approximate the binding time very well. However, even a short excursion into the pausing states can lead to a pause or a change of direction if a state (n_+, n_-) with velocity of zero or different sign is reached. Neglecting these possible pathways for ending a run therefore leads to Eqs. (S18,S19) being overestimates of the run times.
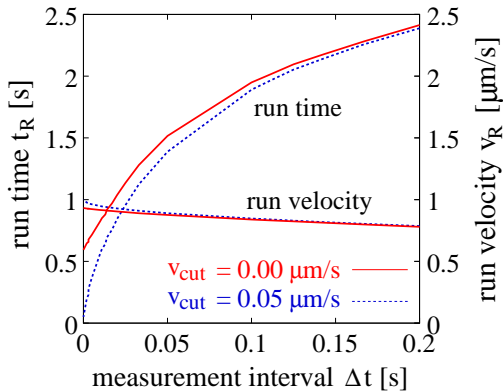
Figure S2: Influence of experimental resolution on run time t_R and run velocity v_R for the symmetric tug-of-war of 4 plus and 4 minus motors with kinesin parameters of Table S1. The run time increases with the measurement time interval Δt, while the run velocity decreases with Δt. Increasing the velocity cutoff v_{cut} from zero (red solid lines) to $0.05\,\mu$m/s (blue dotted lines) has the opposite effects.

S3   Experimental resolution

In this section we show that the measured values of the run times and velocities depend strongly on the experimental resolution. Since the spatial resolution of modern experiments has approached nanometer precision, the time resolution is often more critical for our purposes. A typical time resolution Δt for experiments on bidirectional cargo transport is the video frame rate of 30 frames per second, i.e. $\Delta t = 0.03\,$s (34, 35), but it can vary as much as from $\Delta t = 0.001\,$s (36) to $\Delta t = 2.2\,$s (37). Because of the finite time resolution and of fluctuations of the cargo inside of the cell, it is often hard to decide whether the cargo is moving slowly or pausing. In experiments, a pause is therefore often operationally defined to be a period of time where the cargo moves with a velocity smaller than some cutoff velocity v_{cut}. Choices for v_{cut} are in the range of $0.05\,\mu$m/s (34, 35) or $0.1\,\mu$m/s (37). Fig. S2 shows the effect of the time measurement interval Δt and the velocity cutoff v_{cut} on the run times and velocities for the symmetric tug-of-war.

An increase in the velocity cutoff v_{cut} defines more periods of motion as a 'pause', which decreases the measured run time t_R, see Fig. S2, because a run ends whenever a pause starts. It also increases the run velocity slightly because some slow motion periods are no longer included in the runs.

The main effect of a finite time resolution is that short runs or pauses of duration smaller than the measurement time interval Δt cannot be detected. This leads to longer run times for higher Δt, see Fig. S2, as e.g. a short pause ending a run, or a short minus run interrupting a plus run, remain unnoticed. In consequence the velocity decreases with the time interval Δt.

Fig. S2 shows that the time resolution of the measurement strongly affects the values of the run time, which increases by a factor of 2 already when the measurement time interval is increased to $\Delta t = 0.04\,$s. The run velocities are only marginally affected. Thus caution is necessary when comparing the results from theory and experiment, and from different experiments. However, the order of magnitude and the qualitative variation of the run times and velocities with the motor parameters remain the same for all relevant resolutions. In the main text, we have used 'infinite' resolution, i.e. zero Δt and zero v_{cut}. Note that 'infinite' time resolution is possible also in our computer simulations because we use the Gillespie algorithm (22).

S4   Possible extensions of our theory

Our theory for cargo transport by motor teams is based on single motor properties as deduced from single molecule experiments. In order to obtain a relatively small number of parameters, we have focused on the most important single motor properties provided by the force-dependent unbinding rate and the force-velocity relationship as in Equations (S1) and (S2). In addition,
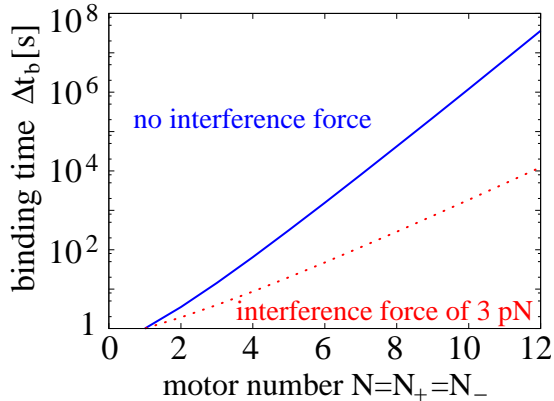
Figure S3: Binding time Δt_b according to Equation (S25) for the stochastic tug-of-war of N plus and N minus motors with kinesin parameters of Table S1 without interference force, i.e. $F_\mathrm{int} = 0$ (blue solid line), and with interference force $F_\mathrm{int} = 3\,\mathrm{pN}$ (red dotted line). Even though the binding time is strongly reduced for $F_\mathrm{int} = 3\,\mathrm{pN}$, i.e., by the presence of the interference force, it still increases exponentially with motor number N as for $F_\mathrm{int} = 0$.

the explicit tug-of-war model described in Section S1 above includes two types of interactions: (i) each motor team can generate load forces on the other motor team; and (ii) same-directional motors share their load equally.

S4.1 Additional motor motor interactions

In general, the motors may experience other types of interactions. In the following, we will briefly describe four such interactions: (i) The chemomechanical cycles of the different motors together with their elastic coupling may lead to effective load forces. Indeed, the motor cycles of two different motors pulling on a cargo are not expected to be synchronized. Consider, e.g., two active motors of the same species. If one of these motors wants to make a relatively fast mechanical step while the other motor undergoes a relatively slow chemical transition, the stepping motor experiences a resisting force arising from the coupling to the other motor. The size of this force depends on the elastic compliance of this coupling. A harmonically coupled pair of motors has been recently studied theoretically in Ref. (38), and the velocity of its center-of-mass was found to be strongly reduced with increasing spring constant; (ii) The motors may experience repulsive interactions from motor crowding and mutual exclusion. For biologically relevant, small motor numbers, these exclusion effects are expected to be relatively small, however, as shown explicitly for cargo transport by one motor team (17); (iii) Another type of interactions arises from hydrodynamics. Such hydrodynamic interactions have been recently studied, to some extent, in Ref. (39), and were also found to have a relatively small effect on cargo transport; and (iv) Effective interactions between the motors may also be mediated via elastic deformations of the filaments as deduced from decoration experiments (40–42) and theoretically considered in Ref. (43). In principle, all of these interactions (i) - (iv) can be included in our theoretical description for a stochastic tug-of-war but will then introduce additional parameters that may be difficult to determine experimentally.

S4.2 Negative motor interference

In a recent in vitro experiment, Rogers *et al.* investigated two kinesins connected by a DNA strand of about $50\,\mathrm{nm}$ (44). The run length of this complex was found to be larger than the run length of a single motor, but shorter than the run length of a complex with two independently moving motors (44). Rogers *et al.* interpreted these observations as evidence for negative motor interference and postulated an effective interference force F_int. This latter force, which was estimated to be of the order of $3\,\mathrm{pN}$ (44), acts as an additional load force on the motors, enhances their unbinding, and thus shortens the run length of the cargo. Although Ref. (44) thus indicates negative interference of same-directional motors linked together by a DNA construct,

other experimental observations on transport of beads by several same-directional motors are consistent with a theoretical description, in which the motors transport the cargo independently (25, 45, 46). On the other hand, it is also not difficult to include interference forces within our theoretical description.

First, consider a single team of one type of motors, say plus motors. In the presence of the interference force F_{int+} acting on each plus motor as proposed in Ref. (44), the unbinding rates $\epsilon_+(n_+, 0)$ as in Equation (S6) for $n_- = 0$ are now given by

$$\epsilon'_+(n_+, 0) = n_+ \, \epsilon_{0+} \, \exp\left[F_{int+}/F_{d+}\right] > n_+ \, \epsilon_{0+} = \epsilon_+(n_+, 0). \tag{S22}$$

which implies increased unbinding and, thus, shorter run lengths.

Second, consider a stochastic tug-of-war between N_+ plus and N_- minus motors. Negative interference of same-directional motors is expected to lead to larger average forces F_+ and F_- on each plus and minus motor, or equivalently to a larger 'cargo force'

$$F'_c(n_+, n_-) > F_c(n_+, n_-) \tag{S23}$$

than given in Equations (S11) and (S13). The precise value and functional form of $F'_c(n_+, n_-)$ will depend on the underlying mechanism for motor interference. If the cargo is transported by both plus and minus motors, $n_+ > 0$ and $n_- > 0$, the larger force $F'_c(n_+, n_-)$ enhances the unbinding cascade of the motors, leading even more quickly to a state in which only one motor type is bound to the filament. However, since opposing motors move into opposite directions and therefore always pull strongly on the other motor type, we expect the forces arising from the interference of same-directional motors to be small compared to the forces of the opposing motors that are taken into account in our model via Equation (S8).

Let us now assume that the interference force between same-directional motors is independent of the number of actively pulling motors. With this assumption, motor interference effectively reduces the motor processivity because the motor unbinding rate is increased from ϵ_{0+} to $\epsilon_{0+} \exp[F_{int+}/F_{d+}]$ as soon as there is more than one motor bound, $n_+ > 1$, see Equation (S22). A calculation similar to the one described in Section S2 leads to an estimate for the plus run time as given by

$$t'_{R,+}(N_+) = \frac{\exp[F_{int+}/F_{d+}]}{N_+ \pi_{0+}} \left[\left(1 + \frac{\pi_{0+}}{\epsilon_{0+} \exp[F_{int+}/F_{d+}]}\right)^{N_+} - 1\right], \tag{S24}$$

to an analogous expression for the minus run time $t'_{R,-}(N_-)$, and to the binding time

$$\Delta t'_b(N_+, N_-) = q_+ \, t'_{R,+}(N_+) + q_- \, t'_{R,-}(N_-). \tag{S25}$$

Using an interference force of $F_{int+} = 3\,\mathrm{pN}$ as deduced by Rogers *et al.* for the interference of two kinesin motors, the unbinding rate of the motors is increased by a factor of $\exp[F_{int}/F_d] \simeq 3$ as soon as more than two motors are bound. As a consequence, the run and binding times of the cargo are drastically reduced, see Fig. S3 for the binding times. Nevertheless, the run and binding times still increase exponentially with the numbers N_+ and N_- of plus and minus motors on the cargo, see Equations (S24) and (S25) and Fig. S3.

In summary, negative motor interference modifies the quantitative, but not the qualitative predictions of our model. The quantitative changes strongly depend on the underlying molecular mechanism.

S5   External forces

In this appendix we consider a generalization of the tug-of-war model presented in Section S1, which described cargo motion in the presence of non-motor forces such as frictional forces $F_{\mathrm{St}} = \gamma_{\mathrm{s}} v_c$ or constant external forces F_{ext}. In this case, the force balance (S8) becomes

$$n_+ F_+ = -n_- F_- + \gamma_{\mathrm{s}} v_c + F_{\mathrm{ext}}. \tag{S26}$$

Remember that the sign of the forces is taken positive in the minus direction, while the sign of the velocity is taken positive in the plus direction.

S5.1   Frictional forces

Validity of Stokes' law. In equation (S26), we have assumed that the frictional force can be described by Stokes' law, $F_{\mathrm{St}} = \gamma_{\mathrm{s}} v_c$, with the friction coefficient $\gamma_{\mathrm{s}} = 6\pi\eta R$ given by the viscosity η of the surrounding medium and the cargo radius R. Stokes' law is valid for the motion of a body in a stationary Newtonian fluid with low Reynolds numbers (47). Since the Reynolds number $\mathrm{Re} = \rho v R/\eta$ for a $1\,\mu$m-sized cargo moving at velocity $v = 1\,\mu$m/s in water with density $\rho = 1\,\mathrm{g/cm}^3$ and viscosity $\eta = 1\,\mathrm{mPa\cdot s}$ equals 10^{-6}, the low Reynolds number limit is clearly fulfilled. Stationarity of the fluid motion is attained on the time scale $T_{\mathrm{fl}} = \rho R^2/\eta$, as follows from dimensional analysis of the Navier-Stokes equation or by explicitly solving the Navier Stokes equation for an oscillating body (47). For water, $T_{\mathrm{fl}} = 10^{-6}\,$s, which means that the surrounding fluid can be considered stationary on the time scales of bidirectional motion, which are the run and switch times and which are of the order of seconds. Thus, on the time scales of our model and for transport in aqueous solution, Stokes' law is valid. *In vivo*, the cytoplasm might cause complications because of obstacles and its non-Newtonian character (48, 49).

    Motor forces and velocities. In the presence of friction but no other external forces, the force balance (S26) with $F_{\mathrm{ext}} = 0$ and the velocity balance (S9) lead to the motor forces

$$\pm F_\pm(n_+, n_-) = F_{s\pm}\, \frac{(1/v_{o+} + 1/v_{o-})\, n_\mp F_{s\mp} + \gamma_{\mathrm{s}}}{n_+ F_{s+}/v_{o+} + n_- F_{s-}/v_{o-} + \gamma_{\mathrm{s}}}\, F_{s\pm} \tag{S27}$$

and to the cargo velocity

$$v_c(n_+, n_-) = \frac{n_+ F_{s+} - n_- F_{s-}}{n_+ F_{s+}/v_{o+} + n_- F_{s-}/v_{o-} + \gamma_{\mathrm{s}}}, \tag{S28}$$

which still fulfills the majority rule (S12). Our simulations for cargo motion in the presence of frictional forces were performed as described in Section S1, using the motor forces and velocities of Equations (S27) and (S28).

    The large-friction-limit. During fast plus motion, only plus motors are pulling, $n_- = 0$. In this case the cargo velocity of Equation (S28) becomes

$$v_c(n_+, 0) = n_+ F_{s+}/\left(n_+ F_{s+}/v_{F+} + \gamma_{\mathrm{s}}\right) \tag{S29}$$

which is Equation (5) in the main text. Since the velocity (S29) depends on the number n_+ of bound plus motors, which can range between 1 and N_+, the velocity distribution displays N_+ peaks for plus-end velocities. In the limit of a large friction coefficient γ_{s}, these peaks are at

$$v_c(n_+, 0) \approx n_+ F_{s+}/\gamma_{\mathrm{s}}, \tag{S30}$$

i.e. at integer multiples of $F_{s+}/\gamma_{\mathrm{s}}$. Note that this has been derived from a decreasing single-motor force-velocity curve (S2). In Ref. (50), it was argued that a velocity dependence on motor

number of the form (S30) should be inconsistent with a single-motor force-velocity-curve (S2). Equation (S30) implies that the velocity of the cargo, and therefore also of each bound motors, increases with the number n_+ of bound motors. At the same time, Equation (S30) implies that the force on a single motor is $F_+ \approx \gamma_s v_c(n_+, 0)/n_+ = F_{s+}$, independent of the number n_+ of bound plus motors. This is apparently inconsistent with a single-motor force-velocity relation (S2) with decreasing force F_+ for increasing velocity v_c. In addition, $F_+ = F_{s+}$ would mean that a single motor experiences a force equal to its stall force, which would lead to zero cargo velocity, $v_c = 0$. The apparent contradictions arise because of the expansion in the small parameter $1/\gamma_s$ for large γ_s. While the first term in the velocity expansion (S30) is of the order of $1/\gamma_s$, the first term in the force expansion $F_+ = F_{s+}$ is of order 1, i.e. independent of $1/\gamma_s$. One therefore has to expand the force (S27) to the next term, leading to the single motor force

$$F_+(n_+, 0) \approx F_{s+} \left[1 - F_{s+} n_+ / (\gamma_s v_{F+}) \right], \tag{S31}$$

which indeed decreases with increasing motor number and therefore also with increasing velocity $v_c(n_+, 0)$.

Friction in cells. The cytoplasm is a complicated medium with high crowding due to proteins and filament meshworks with viscoelastic properties (48, 49). For our purpose this can be accounted for by using an apparent viscosity which depends on the particle size: large particles feel a higher viscosity than small ones. This is related to the observation of slowed diffusion in the cytoplasm compared to diffusion in water (48): For small particles with radii smaller than $50\,\text{nm}$, diffusion is decreased by about a factor of 10, while for particles with radii of $0.1 - 1\,\mu\text{m}$, it is slowed down by a factor of 100 or even 1000. We define the apparent cytoplasmic viscosity η via

$$\eta \equiv k_{\text{B}}T / (6\pi RD), \tag{S32}$$

compare Equation (4) in the main text. Here we assume that the diffusion coefficients D measured for diffusion in the cytoplasm also apply to motor transport, which is however under debate in the literature. While some argue that the viscosities at different intracellular locations might significantly differ (51), others apply the viscosity measured from cytoplasmic diffusion to motor transport in a similar way to us (52, 53). Equation (S32) and the observed slow-down of diffusion in cells mean that the cytoplasmic viscosity for typical cargos of size $R = 0.1 - 1\,\mu\text{m}$ is about 100-1000 times the viscosity of water. Indeed, a cytoplasmic viscosity of the order of $1\,\text{Pa} \cdot \text{s}$, i.e. 1000 times the viscosity of water, has been reported (52, 53).

S5.2 Forces exerted by an optical trap

We now consider the motion of a cargo pulled by two teams of opposing motors in an optical trap. Such an external force can exert opposing as well as assisting force on the motors. We therefore have to extend our single motor force-velocity-curve (S3) to assisting forces:

$$v(F) = v_o(\nu_{\text{FA}} - F/F_s) \qquad \text{for } F < 0. \tag{S33}$$

Here we have extended the definition of the velocity parameter v_o of Equation (S4) to

$$v_o \equiv v_{\text{A}} \text{ for } F < 0, \tag{S34}$$

and defined the parameter ν_{FA} to be equal to v_F/v_{A} for forward motion under assisting force, and to 1 else. We use the value $v_{\text{A}} = 0.1\,\mu\text{m/s}$, which leads to a modest increase of the forward velocity with assisting load, in agreement with single molecule experiments (9, 18).

We also need an expression for the motor unbinding rate (S1) under assisting forces. To our knowledge, no experimental data for motor unbinding in this force-regime is available. Using Kramers rate theory, the unbinding rate should increase exponentially with the absolute value of the assisting force. Although the force scale for this exponential increase could be different from the force scale F_d of the exponential increase (S1) with the load force, we expect it to be of similar order of magnitude. Therefore, and in order to avoid an extra parameter with lack of experimental data, we use the same force scale F_d for both forward and backward load forces:

$$\epsilon(F) = \epsilon_0 \exp\left[|F|/F_d\right]. \tag{S35}$$

Motor forces and velocities. If there is no frictional force, $F_{\text{St}} = 0$, the force balance (S26) and the velocity balance (S9) determine the motor forces

$$\pm F_{\pm} = F_{s\pm} \frac{\left(\frac{\nu_{\text{FA}+}}{v_{o+}} + \frac{\nu_{\text{FA}-}}{v_{o-}}\right) n_{\mp} F_{s\mp} + F_{\text{ext}}/v_{o\pm}}{n_+ F_{s+}/v_{o+} + n_- F_{s-}/v_{o-}} \tag{S36}$$

and the motor velocity

$$v_c(n_+, n_-) = \frac{n_+ F_{s+} - n_- F_{s-} - F_{\text{ext}}}{n_+ F_{s+}/v_{o+} + n_- F_{s-}/v_{o-}}. \tag{S37}$$

The parameters $v_{o\pm}$ and $\nu_{\text{FA}\pm}$ are chosen according to:

$$
\begin{array}{lll}
-n_- F_{s-} \frac{v_{B-} + v_{F+}}{v_{B-}} & \geq \quad F_{\text{ext}}, & \text{plus motors win and feel assisting force} \\[4pt]
-n_- F_{s-} \frac{v_{B-} + v_{F+}}{v_{B-}} & \leq \quad F_{\text{ext}} \leq n_+ F_{s+} - n_- F_{s-}, & \text{plus motors win and feel load force} \\[4pt]
+n_+ F_{s+} \frac{v_{B+} + v_{F-}}{v_{B+}} & \geq \quad F_{\text{ext}} \geq n_+ F_{s+} - n_- F_{s-}, & \text{minus motors win and feel load force} \\[4pt]
+n_+ F_{s+} \frac{v_{B+} + v_{F-}}{v_{B+}} & \leq \quad F_{\text{ext}}, & \text{minus motors win and feel assisting force}
\end{array}
$$

Note that the cargo direction still follows from an intuitive majority rule:

$$
\begin{array}{l}
v_c > 0, \text{ if } F_{s+} n_+ - F_{s-} n_- > F_{\text{ext}} \text{ (plus win)} \\
v_c < 0, \text{ if } F_{s+} n_+ - F_{s-} n_- < F_{\text{ext}} \text{ (minus win)} \\
v_c = 0, \text{ if } F_{s+} n_+ - F_{s-} n_- = F_{\text{ext}} \text{ (tie)}
\end{array}
\tag{S38}
$$

For constant external force $F_{\text{ext}} =$ const, the simulation was performed as described in Section S1, using the motor forces and velocities of Equations (S36) and (S37). For varying external force, we simulated the motion of 10000 cargos and varied the external force during the simulation time. Starting with a force $F_{\text{ext}} = -8\,\text{pN}$, the force was increased by an amount of $+1\,\text{pN}$ every $0.5\,\text{s}$ (rate $2\,\text{pN/s}$) or every $1\,\text{s}$ (rate $1\,\text{pN/s}$). For each value of F_{ext}, the cargo velocity was averaged over the 10000 trajectory velocities at this force value to give the average cargo velocity $\langle v_c \rangle$.

Cargo unbinding. In our calculation, we have neglected cargo unbinding. This is unproblematic for cargos not subject to external forces, compare the discussion in Section 3.2. External forces, though, enhance cargo unbinding, since the motor unbinding rate (S6) increases exponentially with the force on the motors. However, our results for cargos subject to external forces remain valid if the experiments are terminated once a cargo unbinds.

References

1. Müller, M. J. I., S. Klumpp, and R. Lipowsky, 2008. Tug-of-war as a cooperative mechanism for bidirectional cargo transport by molecular motors. Proc. Natl. Acad. Sci. USA 105:4609–4614.

2. Müller, M. J. I., S. Klumpp, and R. Lipowsky, 2008. Motility states of molecular motors engaged in a stochastic tug-of-war. J. Stat. Phys. 133:1059–1081.

3. Schnitzer, M. J., K. Visscher, and S. M. Block, 2000. Force production by single kinesin motors. Nat. Cell Biol. 2:718–723.

4. van Kampen, N. G., 1992. Stochastic processes in physics and chemistry. Elsevier, Amsterdam.

5. Bell, G. I., 1978. Models for the specific adhesion of cells to cells. Science 200:618–627.

6. Svoboda, K., and S. M. Block, 1994. Force and velocity measured for single kinesin molecules. Cell 77:773–784.

7. Kojima, H., E. Muto, H. Higuchi, and T. Yanagida, 1997. Mechanics of single kinesin molecules measured by optical trapping nanometry. Biophys. J. 73:2012–2022.

8. Visscher, K., M. J. Schnitzer, and S. M. Block, 1999. Single kinesin molecules studied with a molecular force clamp. Nature 400:184–189.

9. Carter, N. J., and R. A. Cross, 2005. Mechanics of the kinesin step. Nature 435:308–312.

10. Nishiyama, M., H. Higuchi, and T. Yanagida, 2002. Chemomechanical coupling of the forward and backward steps of single kinesin molecules. Nat. Cell Biol. 4:790–797.

11. Kojima, H., M. Kikumoto, H. Sakakibara, and K. Oiwa, 2002. Mechanical properties of a single-headed processive motor, inner-arm dynein subspecies-c of Chlamydomonas studied at the single molecule level. J. Biol. Phys. 28:335–345.

12. Mallik, R., B. C. Carter, S. A. Lex, S. J. King, and S. P. Gross, 2004. Cytoplasmic dynein functions as a gear in response to load. Nature 427:649–652.

13. Liepelt, S., and R. Lipowsky, 2007. Kinesin's network of chemomechanical motor cycles. Phys. Rev. Lett. 98:258102.

14. Tsygankov, D., and M. E. Fisher, 2007. Mechanoenzymes under superstall and large assisting loads reveal structural features. Proc. Natl. Acad. Sci. USA 104:19321–19326.

15. Thomas, N., Y. Imafuku, and K. Tawada, 2001. Molecular motors: thermodynamics and the random walk. Proc. R. Soc. Lond. B 268:2113–2122.

16. Fisher, M. E., and A. B. Kolomeisky, 2001. Simple mechanochemistry describes the dynamics of kinesin molecules. Proc. Natl. Acad. Sci. USA 98:7748–7753.

17. Klumpp, S., and R. Lipowsky, 2005. Cooperative cargo transport by several molecular motors. Proc. Natl. Acad. Sci. USA 102:17284–17289.

18. Block, S. M., C. L. Asbury, J. W. Shaevitz, and M. J. Lang, 2003. Probing the kinesin reaction cycle with a 2D optical force clamp. Proc. Natl. Acad. Sci. USA 100:2351–2356.

19. Fisher, M. E., and Y. C. Kim, 2005. Kinesin crouches to sprint but resists pushing. Proc. Natl. Acad. Sci. USA 102:16209–16214.

20. Kim, Y. C., and M. E. Fisher, 2005. Vectorial loading of processive motor proteins: implementing a landscape picture. J. Phys. Cond. Matter 17:S3821–S3838.

21. Lipowsky, R., and S. Liepelt, 2008. Chemomechanical coupling of molecular motors: Thermodynamics, network representations, and balance conditions. J. Stat. Phys. 130:39-67.

22. Gillespie, D. T., 1976. A general method for numerically simulating the stochastic time evolution of coupled chemical reactions. J. Comp. Phys. 22:403–434.

23. King, S. J., and T. A. Schroer, 2000. Dynactin increases the processivity of the cytoplasmic dynein motor. Nat. Cell Biol. 2:20–24.

24. Leduc, C., O. Campàs, K. Zeldovich, A. Roux, P. Jolimaitre, L. Bourel-Bonnet, B. Goud, J.-F. Joanny, P. Bassereau, and J. Prost, 2004. Cooperative extraction of membrane nanotubes by molecular motors. Proc. Natl. Acad. Sci. USA 101:17096–17101.

25. Beeg, J., S. Klumpp, R. Dimova, R. S. Gracià, E. Unger, and R. Lipowsky, 2008. Transport of beads by several kinesin motors. Biophys. J. 94:532–541.

26. Vale, R. D., T. S. Funatsu, D. W. Pierce, L. Romberg, Y. Harada, and T. Yanagida, 1996. Direct observation of single kinesin molecules moving along microtubules. Nature 380:451 – 453.

27. Toba, S., T. M. Watanabe, L. Yamaguchi-Okimoto, Y. Y. Toyoshima, and H. Higuchi, 2006. Overlapping hand-over-hand mechanism of single molecular motility of cytoplasmic dynein. Proc. Natl. Acad. Sci. USA 103:5741–5745.

28. Mallik, R., D. Petrov, S. A. Lex, S. J. King, and S. P. Gross, 2005. Building complexity: an in vitro study of cytoplasmic dynein with in vivo implications. Curr. Biol. 15:2075–2085.

29. Reck-Peterson, S. L., A. Yildiz, A. P. Carter, A. Gennerich, N. Zhang, and R. D. Vale, 2006. Single-molecule analysis of dynein processivity and stepping behavior. Cell 126:335–348.

30. Müller, M. J. I., 2008. Bidirectional transport by molecular motors. PhDThesis, University of Potsdam, available at: http://opus.kobv.de/ubp/volltexte/2008/1871/.

31. Wang, Z., S. Khan, and M. P. Sheetz, 1995. Single cytoplasmic dynein molecule movements: characterization and comparison with kinesin. Biophys. J. 69:2011–2023.

32. Qian, H., 2000. A simple theory of motor protein kinestics and energetics. Biophys. Chem. 83:3543.

33. Press, W. H., S. A. Teukolsky, W. T. Vetterling, and B. P. Flannery, 2002. Numerical recipes in C++ : the art of scientific computing. Cambridge University Press, New York.

34. Gross, S. P., M. C. Tuma, S. W. Deacon, A. S. Serpinskaya, A. R. Reilein, and V. I. Gelfand, 2002. Interactions and regulation of molecular motors in Xenopus melanophores. J. Cell Biol. 156:855–865.

35. Gross, S. P., M. A. Welte, S. M. Block, and E. F. Wieschaus, 2002. Coordination of opposite-polarity microtubule motors. J. Cell Biol. 156:715–724.

36. Kural, C., H. Kim, S. Syed, G. Goshima, V. Gelfand, and P. R. Selvin, 2005. Kinesin and dynein move a peroxisome in vivo: a tug-of-war or coordinated movement? Science 308:1469–1472.

37. Pilling, A. D., D. Horiuchi, C. M. Lively, and W. M. Saxton, 2006. Kinesin-1 and dynein are the primary motors for fast transport of mitochondria in Drosophila motor axons. Mol. Biol. Cell 17:2057–1068.

38. Keller, C., 2009. Coupled molecular motors. Diploma Thesis, Humboldt University Berlin, Germany.

39. Korn, C. B., S. Klumpp, R. Lipowsky, and U. S. Schwarz, 2009. Stochastic simulations of cargo transport by several processive molecular motors. J. Chem. Phys. 131:245107.

40. Woodrum D. T., S. A. Rich , and T. D. Pollard, 1975. Evidence for biased bidirectional polymerization of actin-filaments using heavy-meromyosin prepared by an improved method. J. Cell Biol. 67:231-237.

41. Orlova A., and E. H. Egelman, 1997. Cooperative rigor binding of myosin to actin is a function of F-actin structure. J. Mol. Biol. 265:469–474.

42. Vilfan A., and E. Frey, and F. Schwabl, and M. Thormählen, and Y.-H. Song, and E. Mandelkow, 2001. Cooperative rigor binding of myosin to actin is a function of F-actin structure. J. Mol. Biol. 312:1011–1026.

43. Klumpp, S., and R. Lipowsky, 2004. Phase transitions in systems with two species of molecular motors. Europhys. Lett. 66:90–96.

44. Rogers, A. R., J. W. Dreiver, P. E. Constantinou, D. K. Jamison, and M. R. Diehl, 2009. Negative interference dominates collective transport of kinesin motors in the absence of load. Phys. Chem. Chem. Phys. 11:4882–4889.

45. Vershinin, M., B. C. Carter, D. S. Razafsky, S. J. King, and S. P. Gross, 2007. Multiple-motor based transport and its regulation by Tau. Proc. Natl. Acad. Sci. USA 104:87–92.

46. Bottier, C., J. Fattaccioli, M. C. Tarhan, R. Yokokawa, F. O. Morin, B. Kim, D. Collard, and H. Fujita, 2009. Active transport of oil droplets along oriented microtubules by kinesin molecular motors. Lab chip 9:1694–1700.

47. Landau, L. D., and E. M. Lifshitz, 1987. Fluid Mechanics, Second Edition: Volume 6 (Course of Theoretical Physics). Pergamon Press, London.

48. Luby-Phelps, K., 2000. Cytoarchitecture and physical properties of cytoplasm: volume, viscosity, diffusion, intracellular surface area. Int. Rev. Cytol. 192:189–221.

49. Kasza, K. E., A. C. Rowat, J. Liu, T. E. Angelini, C. P. Brangwynne, G. H. Koenderink, and D. A. Weitz, 2007. The cell as a material. Curr. Opin. Cell Biol. 19:101–107.

50. Martinez, J. E., M. D. Vershinin, G. T. Shubeita, and S. P. Gross, 2007. On the use of in vivo cargo velocity as a biophysical marker. Biochem. Biophys. Res. Comm. 353:835–840.

51. Gross, S. P., M. Vershinin, and G. T. Shubeita, 2007. Cargo transport: two motors are sometimes better than one. Curr. Biol. 17:R478–R486.

52. Hill, D. B., M. J. Plaza, K. Bonin, and G. Holzwarth, 2004. Fast vesicle transport in PC12 neurites: velocities and forces. Eur. Biophys. J. 33:623–632.

53. Shtridelman, Y., T. Cahyuti, B. Townsend, D. DeWitt, and J. C. Macosko, 2008. Force-velocity curves of motor proteins cooperating in vivo. Cell Biochem. Biophys. 52:19–29.